



## Full Length Article

An insight on the origin of half-metallicity of new equiatomic quaternary Heusler alloys PtRuTiZ ( $Z = \text{Al/Si}$ ): GGA and GGA + U approachesKunal Labar<sup>a,b</sup>, A. Shankar<sup>b,\*</sup>, M. Das<sup>b</sup>, Ranjan Sharma<sup>a</sup><sup>a</sup> Department of Physics, Cooch Behar Panchanan Barma University, Cooch Behar, West Bengal 736101, India<sup>b</sup> Condensed Matter Theory Research Lab, Department of Physics, Kurseong College, Kurseong, Darjeeling 734203, India

## ARTICLE INFO

**Keywords:**  
 Half-metal  
 Heusler alloys  
 FP-LAPW  
 GGA  
 GGA+U  
 Energy bands

## ABSTRACT

In this paper, we have presented a comparative investigation of a new equiatomic quaternary Heusler alloy PtRuTiZ ( $Z = \text{Al and Si}$ ) under the GGA and GGA + U schemes and search for its possibility as a half-metallic material for spintronic devices. These alloys, which crystallize in a magnetic phase of LiMgPdSn (Y-type) structure with space group F-43 m, are thermodynamically and mechanically stable. The electronic properties predict these materials to be half metal under the GGA + U scheme considering the strong exchange splitting among the  $d$ -orbital of transition metals with a half-metallic gap of 0.07 eV and 0.1 eV for PtRuTiAl and PtRuTiSi, respectively signifying their prospect in power electronic applications. Here, PtRuTiSi is rigid and stiffer than PtRuTiAl and their magnetic properties also follow the Slater – Pauling rule of  $M_T = Z_T - 24$  under the GGA + U scheme. The high range of pressure that PtRuTiSi (-1 GPa to 14 GPa) can retain its half-metallic behavior as compared to PtRuTiAl (-3 GPa to 4 GPa) may be linked to their bulk modulus.

## 1. Introduction

Half metal (HM), best known for its 100 % spin-polarized nature between the majority and the minority spin channels at the Fermi energy level ( $E_F$ ), has a functional contribution to spintronic devices. Among the various classes of half-metals, the Heusler alloys (HA) have proven themselves to be an efficient candidate [1] for successful applications in spintronic devices, such as spin valves [2], spin filters [3], spin injectors [4], and magnetic tunnel junctions (MTJ) [5]. The observed half-metallic electronic and magnetic properties, flexible composition with tuneable nature, and comparatively low power dissipation capability due to resistive scattering disorder [6] of equiatomic quaternary Heusler (EQH) alloys have attracted much attention among the family of HAs. In addition to novel half-metallic properties, some of these alloys are also found to possess spin-gapless semiconducting (SGS) nature [7], efficient thermoelectric behavior [8], and semi-metallic properties [9], which make the field of study more versatile. In the EQH alloy with empirical formula  $XX'YZ$ , [10,11] where X, X', Y are the  $d$ -transition metal and Z is the  $s-p$  block element of the periodic table. The exchange splitting between these  $d$ -orbital transition elements governs the tuneable half-metallic properties [12]. Here, the choice of constituent element Z also affects the hybridization between the atoms and improves the

magnetic moment and therefore enhances their overall magnetic profile. For example, when Al is replaced by Si in FeCrRuZ [13], FeMnScZ [14], CoFeMnZ [15], and ZrCoTiZ [16], the extra  $p$ -electron of Si increases the effective  $d$ -charge of these alloys, and thus improves their overall magnetic moment.

The theoretical approach to modelling these magnetic intermetallic alloys and their correlation with experimental outcomes strongly depends on the exchange–correlation approximations used in the first principle calculation. In this respect, the generalized gradient approximation (GGA) [17] schemes are commonly preferred to study magnetic Heusler materials having weak or intervening electronic correlations. Here, it is noteworthy that the GGA-estimated optimized lattice constants are in close agreement with the corresponding experimental reports of Heusler alloys [12,18,19]. Furthermore, this approximation has successfully explained the origin of half-metallic behavior [20] with total magnetic moments equal to the value as predicted by Slater-Pauling (SP) rule [12]. However, the inclusion of GGA approximations has shortcomings in the inadequacy of proper representation of the exchange–correlation functional attributing for strongly correlated systems comprising of localized  $d$  orbital, which thereby over-delocalize the wave functions [21,22]. Therefore, it is necessary to adequately approximate the effect of on-site Coulomb and exchange interactions for

\* Corresponding author.

E-mail address: amitshan2009@gmail.com (A. Shankar).

magnetic materials comprising the partially filled  $d$ -orbital transition metals by adding the Coulomb repulsion ( $U$ ) term in the calculation [23]. In doing so, the unwanted delocalized states found near the Fermi energy level [ $E_F$ ] due to the interaction of the transition metals [22] can be avoided. It is observed that the addition of  $U$  with exchange-correlation functional considerably increases the splitting of  $d$ -states, thereby pushing the Fermi energy level and formation of energy gap at minority spin channel with an overall half-metallic nature to the Heusler alloys [21]. A distinct effect of  $U$  has been also reported in mixed  $d$ -orbital based Heuslers [24–28], where the inclusion of  $U$  in GGA (GGA +  $U$ ) can explain the origin of half-metallicity. Similarly, GGA +  $U$  also confirms the experimental report of half-metallic CoRhTiAl [29]. The theoretical studies on the mixed  $d$ -orbital based EQH alloys like (Ni/Pd/Ru)ZrTiAl [25] and FeVRuSi [26] also predict their half-metallic nature under the purview of the GGA +  $U$  approximation.

Venkateswara *et al.* [30] have suggested that a disorder in the crystal, which may destroy its half-metallicity can be minimized by choosing the constituent elements  $X$  and  $X'$  with higher electronegativity belonging to  $4d$  or  $5d$ -orbitals compared to the  $Y$  in the  $XX'YZ$  structure of EQH alloys. Furthermore, the nature of interactions between the  $d$ -orbitals of  $X$  and  $X'$  hybridizing with the  $Y$  atoms suggests the tentative gap formation in the  $E_F$  [12], along with the tendency of the  $Z$  to increase the overall magnetic profile. Hence, in the present study, we have chosen the mixed  $d$ -orbital based EQH alloy PtRuTiZ ( $Z = Al$  and  $Si$ ) constituted by two heavy transition metals Pt and Ru with higher electronegativity as compared to Ti for our study. The first principles calculations of the electronic, elastic, and magnetic properties of the sample PtRuTiZ ( $Z = Al$  and  $Si$ ) are carried out by using GGA and GGA +  $U$  schemes to predict their exact ground state and understand the origin of half-metallic nature.

## 2. Computational details

A first principle technique was implemented to investigate the compounds using the full-potential linearized augmented plane-wave (FP-LAPW) method under the purview of the wien2k code [31]. The exchange-correlation functional is treated using the generalized gradient approximation (GGA) under the Perdew–Burke–Ernzerhof (PBE) scheme [17]. The effect of strongly localized  $d$ - $d$  exchange interaction of transition metals was treated by including the on-site Coulomb interaction term  $U$  [21] in the calculation along with PBE-GGA (GGA +  $U$ ) which adds an intra-atomic Hubbard interaction ( $U$ ) in the energy functional. The  $U$  values used are 3 eV, 3 eV, and 4.4 eV for Pt, Ru, and Ti, respectively, using Duradev's approach [33]. The shape approximation of the potential well for a crystal lattice is explained by the muffin tin (MT), and the Fourier series is used to express the interstitial region of MT, where the wave functions of the MT spheres are used to approximate the spherical harmonic functions. The radii of the MT spheres are calculated as 2.5 a.u., 2.49 a.u., 2.38 a.u., 2.26 a.u., and 2.06 a.u. for Pt, Ru, Ti, Al, and Si, respectively. The cut-off energy for  $K_{max} \times R_{MT}$  is set to 8.0 Ry, where  $K_{max}$  is the largest reciprocal lattice vector in the plane wave representation. The  $G_{max}$  representing the wave vector in the Fourier series of the charge density and potential in the interstitial region was set to 13a.u.<sup>-1</sup>. The energy convergence criterion was set to  $10^{-4}$  Ry, and the energy cut-off was set to  $-6$  Ry to separate the core and the valence region. A dense mesh of  $14 \times 14 \times 14$  grid k-points was used to integrate over the Brillouin zone (BZ) following the convention of Monkhorst and Pack [32].

## 3. Results and discussion

### 3.1. Structural stability and elastic properties

PtRuTiZ ( $Z = Al$  and  $Si$ ) crystallizes in LiMgPdSn (Y-type) structure with space group F-43 m where Pt, Ru, Ti, and Z are positioned at the Wyckoff's position 4a (0,0,0), 4b (0.5,0.5,0.5), 4c (0.25,0.25,0.25), and

4d (0.75,0.75,0.75) [12,13], respectively as shown in Fig. 1. In the previous report, the isostructural compounds like FeMnScZ ( $Z = Al$ ,  $Ge$ ,  $In$ ) [14], FeMnTaAl [35] and its structural invariance with the EQH alloy  $XX'YZ$  ( $X = Co$ ,  $Ni$ ;  $X' = Fe$ ;  $Y = Ti$ ;  $Z = Si$ ,  $Ge$ ,  $As$ ) [36], ScFeRhP [37], CoFeMnZ ( $Z = Al$ ,  $Ge$ ,  $Si$ ,  $Ge$ ) [38], CoFeMnSi [39] was also found to crystallize in F-43 m phase space. The crystal structure of PtRuTiZ was optimized by fitting the volume and the corresponding total energy into Murnaghan's equation of state [34] for the magnetic and non-magnetic configuration of the system as shown in Fig. 1. The optimized lattice constants corresponding to the minimum total energy of the system, as given in Table 1, are also consistent with analogous PtVScAl (6.369 Å), PtVYAl (6.608 Å), PtVYGa (6.600 Å), FeCrHfAl (6.142 Å), OsCrZrAl (6.347 Å) [40]. From Fig. 1b, one can also note that these alloys have a magnetic ground state where the addition of Si shrinks the volume of the crystal. A similar observation was also made in analogous CoFeMnZ ( $Z = Al$ ,  $Si$ ) [38], and FeCrRuZ ( $Z = Al$ ,  $Si$ ) [13].

The possibility of experimental synthesis of these theoretically designed materials in the laboratory is demonstrated by its thermodynamic stability defined by formation energy ( $E_{for}$ ), which measures the energy required to break the system into its constituents.  $E_{for}$  of the system calculated using Eq. (1) [27] is the difference between the total energy of the bulk sample and the total of the individual energies of the composing atoms in the bulk state within the unit cell. Here,  $E_{PtRuTiZ}$  is the total energy of PtRuTiZ and similarly,  $E_{Pt}$ ,  $E_{Ru}$ ,  $E_{Ti}$ , and  $E_Z$  are the individual energies of Pt, Ru, Ti, and Z in bulk state, whose values are found to be -5.1963.04 eV, -123310.35 eV, -23227.65 eV, and -6603.93 eV (for Al) / -7887.63 (for Si) respectively. The negative amplitudes of the  $E_{for}$  as summarized in Table 1, predict the thermodynamic stability of the sample alloys in the fcc (F-43 m) structure which further awaits experimental verification. A similar prediction was also made from the results of the  $E_{for}$  for the analogous EQH materials in the literature [41,42].

$$E_{for} = [E_{PtRuTiZ} - (E_{Pt} + E_{Ru} + E_{Ti} + E_Z)]/4 \quad (1)$$

The knowledge of the mechanical properties of spintronic materials is essential for their effectiveness in commercial devices. The independent elastic stiffness tensor ( $C_{ij}$ ), which describes the mechanical parameters and the stability of the crystal, quantifies the material's ability to regain its configuration in a strenuous environment, thereby relating the proportionality between the applied stress and strain [43]. Due to the cubic symmetry of the sample material, the only non-zero elastic coefficients  $C_{11}$ ,  $C_{12}$ , and  $C_{44}$  (see Table 1), estimated by using the volume conservation technique [44], define the elastic strain and follow the criteria of  $C_{11} > 0$ ,  $C_{44} > 0$ ,  $C_{11} - C_{12} > 0$ , and  $C_{11} + 2C_{12} > 0$  for mechanical stability of the samples [45,46].

The independent elastic coefficients can further be used to approximate the bulk modulus ( $B$ ), the Voigt-Reuss-Hill approximation to determine the shear modulus ( $G$ ), Cauchy pressure (CP), Young's modulus ( $E$ ), the Poisson's ratio  $\nu$  given by Eqs. (2)-(6) [42,46] as summarized in Table 1.

$$B = (C_{11} + 2C_{12}) / 3 \quad (2)$$

$$G = (G_V + G_R)/2 \quad (3)$$

$$\text{where } G_V = (C_{11} - C_{12} + 3C_{44})/B = (C_{11} + 2C_{12}) / 3.5 \\ \text{and } G_R = 5C_{44}(C_{11} - C_{12})/\{4C_{44} + 3(C_{11} - C_{12})\}$$

$$CP = C_{12} - C_{44} \quad (4)$$

$$E = 9GB/(3B + G) \quad (5)$$

$$\nu = (3B - 2G)/\{2(3B + G)\} \quad (6)$$

$G_V$  and  $G_R$  are Voigt's and Reuss's shear modulus, respectively. On analysis,  $B$ , which measures the resistivity of a material to fracture, is found to have a comparatively higher value for PtRuTiSi. In contrast, PtRuTiSi has a more rigid nature than PtRuTiAl, as predicted from  $G$ ,

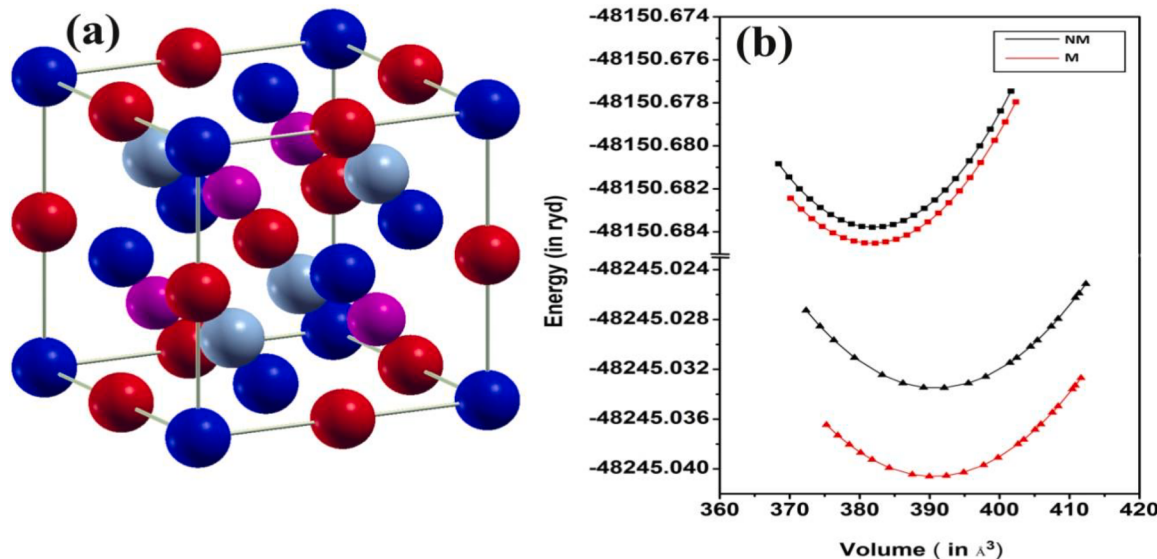


**Fig. 1.** A) the crystal structure for PtRuTiZ ( $Z = \text{Al}, \text{Si}$ ) where Pt (blue), Ru (grey), Ti (red), and Z (purple), and b) volume optimization curve for PtRuTiAl (triangle) and PtRuTiSi (square) for magnetic (M) and non-magnetic (NM) phases. (For interpretation of the references to colour in this figure legend, the reader is referred to the web version of this article.)

**Table 1**

The optimized lattice constant ( $a_0$ ) in  $\text{\AA}$ , formation energy ( $E_{\text{for}}$ ) in eV, independent elastic constants ( $C_{11}$ ,  $C_{12}$ , and  $C_{44}$ ), bulk modulus (B), and isotropic shear modulus (G), Young's modulus (E) in GPa, Poisson's ratio ( $\nu$ ) and Cauchy's Pressure (CP) of PtRuTiZ.

Z	$a_0$	$E_{\text{for}}$	$C_{11}$	$C_{12}$	$C_{44}$	B	G	E	$\gamma$	$\nu$	CP
Al	6.169	-2.30	201.4	199.2	104.4	200	32.0	93.5	0.42	0.42	94.8
Si	6.136	-2.35	574.0	24.2	101.9	207	153.6	369.7	0.20	0.20	-77.7

which defines the material's resistance to plastic deformation. The values obtained in the present calculation are qualitatively equal with analogous CoYCrAl and CoYCrSi [47], CoRhMnAl and CoRhMnSi [48], RXVZ (R = Yb, Lu; X = Fe, Co, Ni; Z = Al, Si) [49]. The calculated values of E, defining the response of the material against lateral strain and thus predicting the stiffness, suggest the highly rigid nature of PtRuTiSi. The Poisson's ratio value of ~0.3 or lower, the materials are less compressible and tend to show more excellent stability to externally applied strain [50]. Hence  $\nu$  value is more significant than the critical value, and PtRuTiAl is less compressible than PtRuTiSi. Furthermore, the negative amplitude of the Cauchy pressure of PtRuTiSi denotes that the material is ductile, whereas PtRuTiAl is brittle.

### 3.2. Electronic structures and half-metallicity

Studying the density of states (DOS) and energy band structures of material can open the electronic and magnetic properties, helpful in contemplating its scope in technological applications. To have a refined analysis of the said properties, we have used the GGA and GGA + U exchange–correlation approximations in the *ab initio* study of our materials. The calculated total DOS and partial DOS representation for GGA and GGA + U are depicted in the figure (Figs. 2 and 3). One can see an analogous occupancy in the density of states for both spin-up and spin-down channels at similar energies in the total DOS (and partial DOS) under GGA approximations for PtRuTiAl and PtRuTiSi, which therefore gives an overall zero magnetic moment profiling to the material. The results thus obtained deviate from the required total spin magnetic

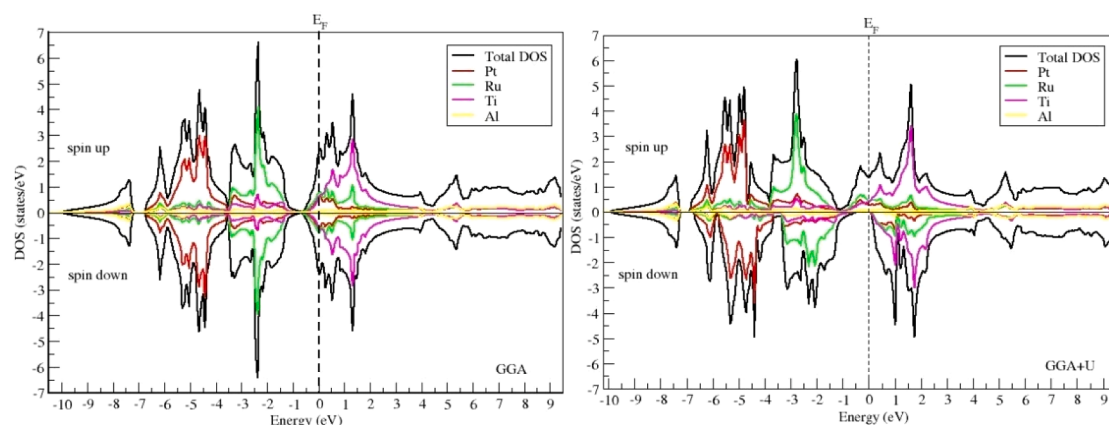


**Fig. 2.** Total and partial density of states of PtRuTiAl.

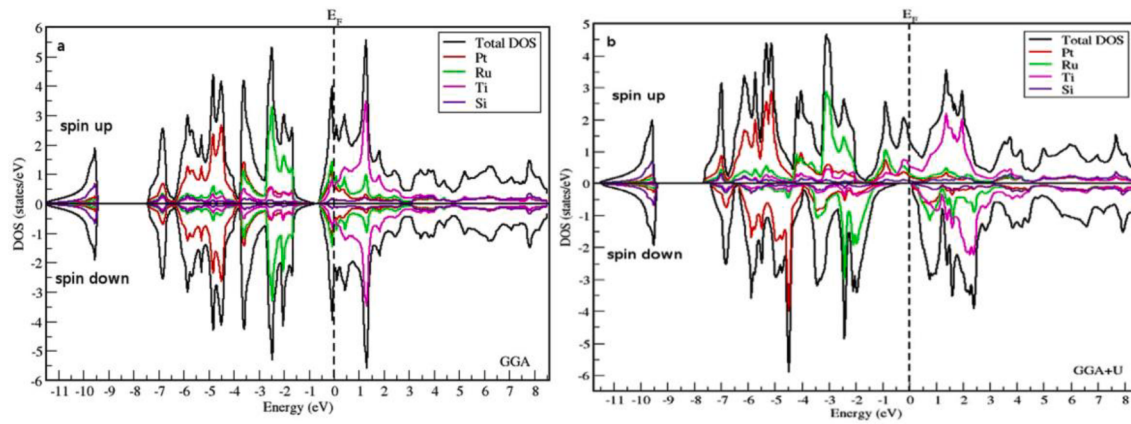


**Fig. 3.** Total and partial density of states of PtRuTiSi.

moment of  $1.00 \mu_B / f.u$  and  $2.00 \mu_B / f.u$  (for PtRuTiAl and PtRuTiSi, respectively), preferable for the half-metallic properties as suggested by the SP rule of  $M_T = Z_T - 24$  [12] relating the total valence electron count  $Z_T$  with the total magnetic moment  $M_T$ . Also, with no band gap in spin down or spin up channel instead gives a metallic nature to the compounds under study. The results obtained may be regarded as the incompetence of the GGA scheme to properly treat the strong on-site Coulomb's interactions present in the transition metals comprising  $d$  and  $f$ -orbitals along with the interactions embedded with the  $s-p$  states. For this, incorporating the U correction is required to correctly correlate the interaction of these localized orbitals along with coupling interaction with the  $s-p$  states for further analysis of their physical properties, as suggested by A. Sarah Tolba *et al.* (2018) [22]. The author suggests the U value in the Hamiltonian of GGA can push away the localized orbital states lying in the bandgap near the EF, further preventing the unwanted delocalized  $d$  orbital electrons formed when two transition metal electrons reside in the same cation [51].

Now, a careful analysis of the energy bands of PtRuTiZ under the GGA + U scheme reveals the semiconducting nature of the minority spin (or spin down) channel and a metallic face in the majority spin (or spin up) channel predicting the material to have 100 % spin polarisation near EF, thereby defining a half-metallic nature to PtRuTiZ. Referring to Figs. 2 and 3, we see that in comparison to the GGA scheme, the  $d$ -orbitals of the Ti element are pushed towards the positive energy beyond the EF when the onsite Coulomb interaction is taken into account under the GGA + U scheme for PtRuTiZ, thus showing a half-metallic nature to the alloys. Similar reports on the influence of the U parameter while

predicting the half metallicity of Heusler alloys [23,24,26–28], indicate the principal role played by the Coulomb's interaction among the transition metal elements. Further investigating in terms of the energy band structure (Figs. 4 and 5) for PtRuTiAl and PtRuTiSi under the GGA + U scheme, in PtRuTiAl, there exists a half-metallic gap or spin-flip gaps (EHM) and semiconducting bandgap (Eg) of 0.07 eV and 0.53 eV, respectively. In contrast, EHM of 0.1 eV and Eg of 0.48 eV are observed in PtRuTiSi. Previous reports on analogous EQH suggest the better performance of wider bandgap materials [52] for power electronic applications and a similar conclusion can be made for the sample alloys with comparatively wider bandgap as compared to CoRhMnSi [11], FeCrRuSi (0.384 eV) [41], CoRuTiGe (0.35 eV) and CoRuTiSn (0.28 eV) [53], FeRhCrSi (0.336 eV) and FePdCrSi (0.177 eV) [54].

Referring to the DOS plots (Figs. 4 and 5), the sharp peaks in both spin channels correlate with the flat bands present in the high symmetric point of the energy band structure. There exist the signature gap towards the core region at both the spin channels measured at 0.4 eV (for PtRuTiAl) and 1.8 eV (for PtRuTiSi) typically seen in any Heusler alloys. This gap arises due to the strong hybridization between the  $s-p$  element Al and Si with the  $d$ -orbital transition metal elements Pt, Ru, and Ti in PtRuTiZ. Focussing the spin-down channel where the band gap is observed, the maximum amplitude of about  $-0.43$  states/eV (at  $-7.33$  eV) is acquired by Al in PtRuTiAl. Similarly, the states acquired by Si is  $-0.72$  states/eV (at  $-9.4$  eV) in PtRuTiSi, which therefore does not affect the gap formation near the EF. The variation in the measure of hybridization between Al and Si can correspond with the inter-atomic distance between the Al (or Si) with the other individual transition

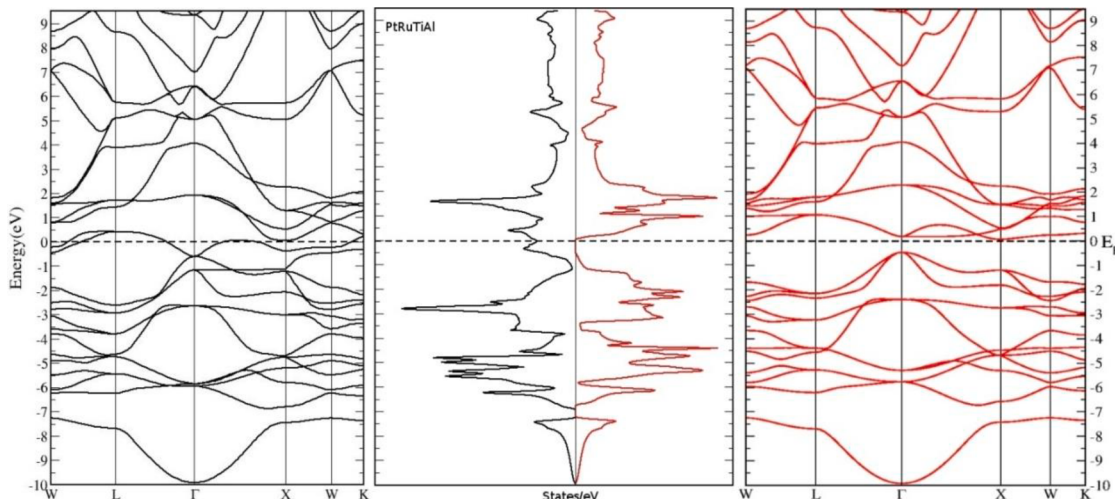


**Fig. 4.** Energy band structure for the spin-up channel (left panel), spin-down channel (right panel), and total density of states (middle panel).

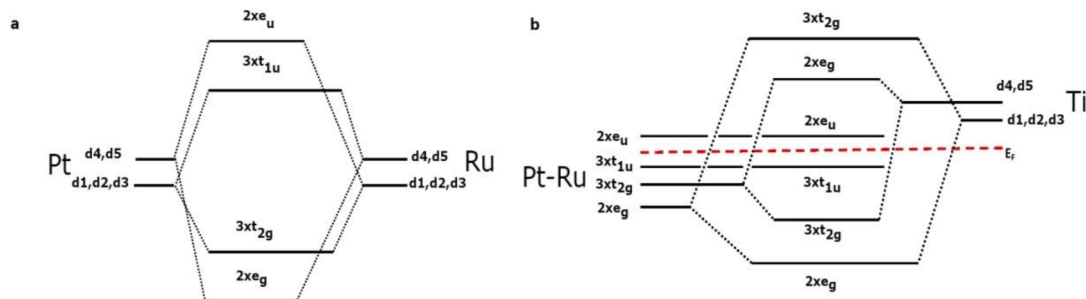


**Fig. 5.** A) hybridization scheme between the five bonding ( $d_1, d_2, d_3, d_4$ , and  $d_5$ ) degenerate states following the tetrahedral symmetry among pt and ru orbitals, and b) hybridization between the pt – ru hybrids and the Ti orbitals.

metals in the unit cell of PtRuTiZ. The inter-atomic distance is found to be 2.67 Å and 3.08 Å between Pt (or Ru) - Al and Ti-Al (in PtRuTiAl), respectively, and 2.65 Å and 3.06 Å between Pt (or Ru) - Si and Ti - Si (in PtRuTiSi), respectively. The inter-atomic distance relating to Al is comparatively higher compared to Si with the other transition metals in the assemblage, thereby showing a reduced hybridization for Al. However, their functionality in decreasing the effective charge of  $d$  orbital transition metal elements further increases the material's stability [12].

The hybridization among the  $d$ -orbital transition metals in the material typically leads to gap formation, as suggested by Ozdogan *et al.*

[12]. Now, understanding the gap formation, we take PtRuTiAl, where we can see the hybridization of Pt and Ru giving two sets of i) five bonding degenerate states ( $2 \times e_g$  and  $3 \times t_{2g}$  hybrid states) following the tetrahedral symmetry and ii) five non-bonding degenerate states ( $2 \times e_u$  and  $3 \times t_{1u}$  hybrid states) in octahedral symmetry (Fig. 6a). Furthermore, the five bonding states of Pt – Ru hybrid states further hybridize with Ti to produce five bonding states giving  $2 \times e_g$  and  $3 \times t_{2g}$  hybrid states of tetrahedral symmetry and five antibonding states. The non-bonding  $2e_u$  and the bonding  $2e_g$  and  $3t_{2g}$  are moved towards the higher energy above  $E_F$ . In contrast, the remaining hybrids  $3t_1$ ,  $3t_{2g}$ , and

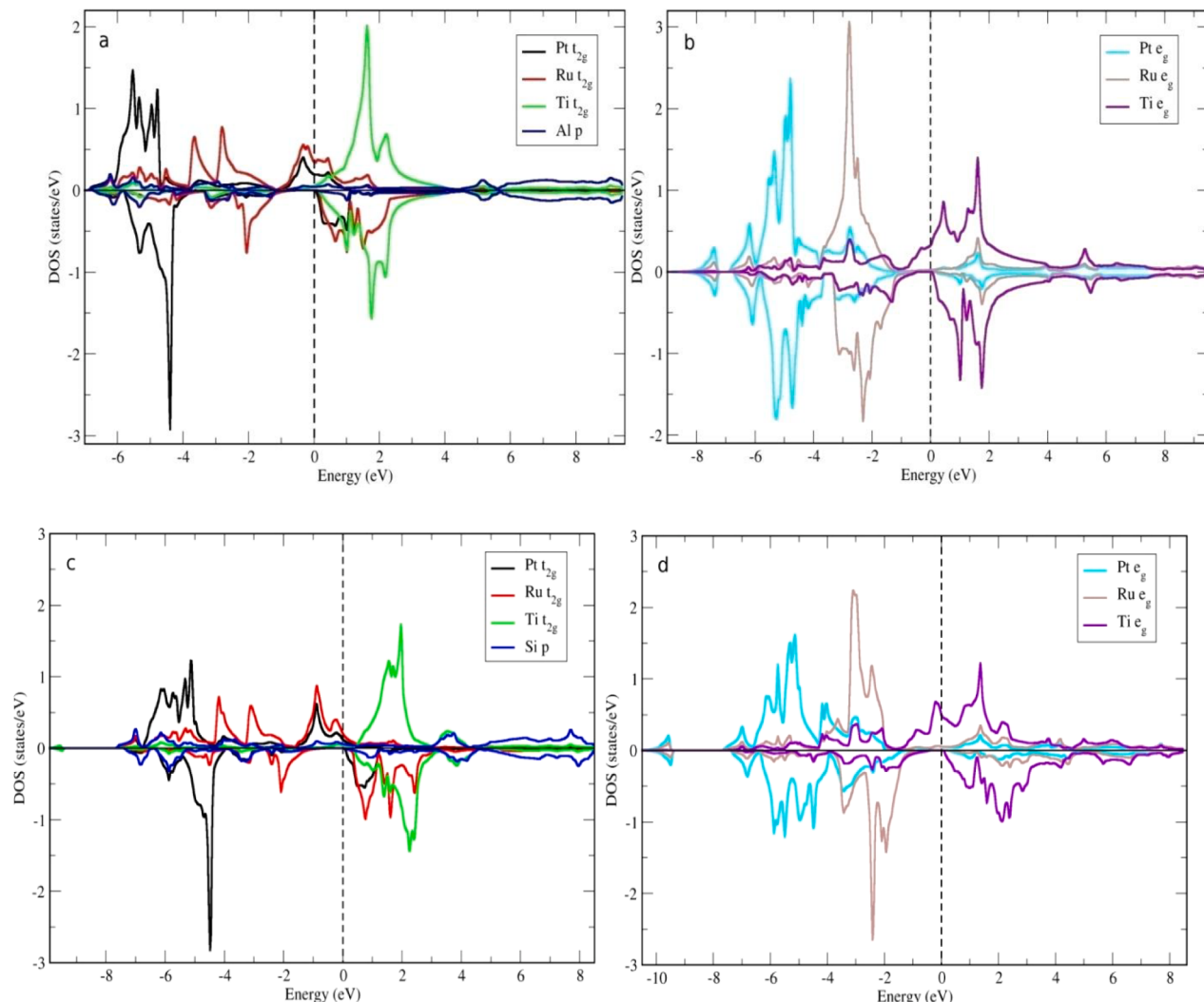


**Fig. 6.** Partial density of states of (a,b) PtRuTiAl and (c,d) PtRuTiSi.

$2e_g$  are pushed down to lower energy below  $E_F$  opening a gap between the states as depicted in the schematic Fig. 6b.

In Fig. 7, the minority spin channel reveals enhanced hybridization among the  $d$  orbital near the EF when the U correction is implemented along with the GGA scheme. The lowest energy region comprises the Pt states headed by the  $t_{2g}$  states of Pt, peaked with  $-2.9$  states/eV (at  $-4.4$  eV) and the  $e_g$  states with  $-1.81$  states/eV (at  $-5.2$  eV). The maximum contribution in the hybrids lying towards the negative energy closer to the EF is mainly by the hybrid states of Ru, where its  $t_{2g}$  states occur closer to the EF level with the  $-0.78$  states/eV (at  $-2$  eV). In contrast, the  $e_g$  states reside with a maximum of  $-1.9$  states/eV (at  $-2.29$  eV). The hybrid states mainly contributed by the Ti are pushed towards the positive energy beyond EF. The presence of  $e_g$  states lies distinctly closer to the EF level marked at  $1.35$  states/eV (at  $1$  eV). This observation shows that with the inclusion of the U term to the Hamiltonian of the system under GGA, the strong exchange splitting among the Pt – Ru hybrids pushes the Ti hybrids towards the conduction region, eventually resulting in the half-metallic gap, thus supporting the idea for the gap formation. This gap exists between the  $e_g$  and the  $t_{2g}$  hybrid orbitals in the hybridization of the transition metals, as discussed earlier (Fig. 6). Similar behavior in hybridization is seen in PtRuTiSi (see Fig. 7c and 7d), where the Ti states are pushed towards the conduction region beyond EF by the hybridized states of Pt-Ru lying in the valence region below the EF.

### 3.3. Magnetic properties

The magnetic properties of PtRuTiZ were analyzed under GGA and GGA + U approximations. Referring to Table 2, both PtRuTiAl and PtRuTiSi have almost zero magnetic moments when calculated under the purview of GGA approximations, along with a metallic nature as supported by the electronic structure. However, the results drastically change both in terms of magnetic and electronic properties in the GGA + U approximations. The influence of 'U' in PtRuTiZ considerably predicts a total spin magnetic moment of  $1.008 \mu_B/\text{f.u}$  for PtRuTiAl and  $1.999 \mu_B/\text{f.u}$  for PtRuTiSi under the GGA + U approximations. The distribution of  $3t_1$ ,  $3t_{2g}$ , and  $2e_g$  states lying below the EF level suggest the occupancy of eight electrons below the EF (refer to Fig. 6b) and adding the occupied electrons from  $s$  and  $p$ , thus giving us twelve valence electrons below the EF. The total magnetic moment  $M_T$  is the resultant between the number of valence electrons in the majority spin channel (NU) and the number of valence electrons in the minority spin channel (ND). In contrast, the total valence number  $Z_T$  is the sum of NU and ND per formula unit, which thereby gives us an equation relating  $M_T$

and  $Z_T$  as  $M_T = Z_T - 2 N_D$ . As discussed, the ND here has been calculated as 12, which in consequence follows the SP rule of  $M_T = Z_T - 24$ . So, with the empirical formula thus obtained, the expected total spin magnetic moment for PtRuTiAl and PtRuTiSi should be  $1 \mu_B/\text{f.u}$  and  $2 \mu_B/\text{f.u}$ , respectively. The close agreement in the calculated numerical data for the total spin magnetic moment with the SP rule substantially upholds the GGA + U approximation predicting that the material is half-metallic. The calculated  $M_T$  for PtRuTiAl and PtRuTiSi suggest the recommendation of GGA + U to ideally represent the material to be half-metallic compared to the other approximations as suggested by the SP rule for the half-metallic nature.

The individual contribution of magnetic moments by the constituent elements headed by Ru in PtRuTiZ suggests its ferromagnetic nature. Furthermore, the Stoner criteria [55] calculated for both the materials (see Table 2) followed the  $N(\text{EF}) \times IF > 1$  benchmark, which supports their ferromagnetic phase, where  $N(\text{EF})$  and  $IF$  are the density of states and stoner parameter, respectively at EF. The data further reveal the maximum contribution in the magnetic moment for the materials to be contributed by Ru. A similar observation was also made in analogous compounds like FeMnTaAl [35], FeCrRuSi [41], and ZrCrCoZ ( $Z = \text{B}, \text{Al}, \text{Ga}, \text{In}$ ) [56]. Analyzing the data in Table 2, the calculated magnetic moment under GGA + U for PtRuTiAl and PtRuTiSi complies with the SP rule.

### 3.4. Effect of pressure

The pressure induced by changed inter-atomic distance varies the lattice constant in the unit cell, impacting the hybridization and magnetic moment of Heusler alloys [57].

In Fig. 8, the variation in the lattice constant, along with its total energy in PtRuTiAl and PtRuTiSi for the induced pressure implies the material's constriction in maintaining its half-metallic limit with the highest negative energy under optimized pressure conditions. Furthermore, the retention in half metallicity between a pressure range from  $-3$  GPa to  $4$  GPa for PtRuTiAl and  $-11$  GPa to  $14$  GPa for PtRuTiSi which can be again verified by referring to Fig. 9, which shows the plot for conduction band (CB) maximum energy and valence band (VB) maximum energy for different pressure applications.

The enhanced retention in the half-metallicity for PtRuTiSi for a wide pressure range compared to PtRuTiAl may be accounted for due to high bulk modulus and shear modulus PtRuTiSi. So, with higher B and G values, the change in the lattice distance under a strenuous environment is comparatively restricted in PtRuTiSi, which further supports keeping the strength of the hybridization along with the required magnetic

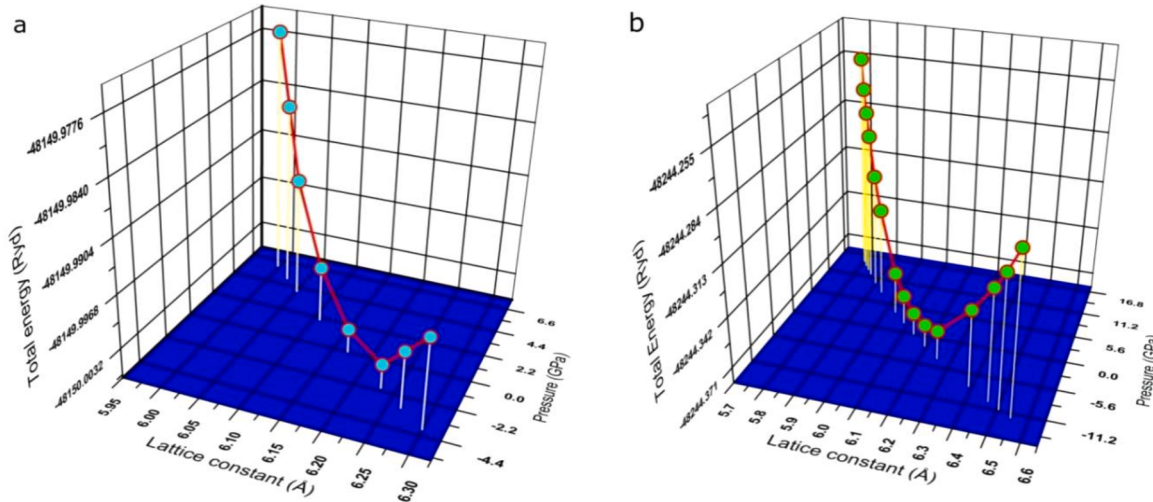


Fig. 7. A) variation of lattice constant with corresponding energy against applied pressure for PtRuTiAl and b) Variation of lattice constant with corresponding energy against applied pressure for PtRuTiSi.

**Table 2**

The individual and total magnetic moment (in  $\mu_B$ /f.u) of PtRuTiAl and PtRuTiSi under the GGA + U scheme, the Stoner criteria of  $I_F \times N(E_F) > 1$ , where  $I_F$  is the Stoner parameter and  $N(E_F)$  is the number density at  $E_F$ .

Compound	S-P rule	Magnetic moment						$I_F$	$N(E_F)$
		Total ( $M_T$ )	Pt	Ru	Ti	Al	Si		
PtRuTiAl	1	1.00	0.227	0.775	0.057	-0.012	-	4.48	0.45
		-0.03*	-0.011*	-0.043*	0.021*	0.000*	-		
PtRuTiSi	2	1.99	0.365	1.048	0.476	-	0.040	3.87	0.33
		0.03*	0.005*	0.016*	0.012*	-	0.000*		

\*Calculation under the GGA scheme.

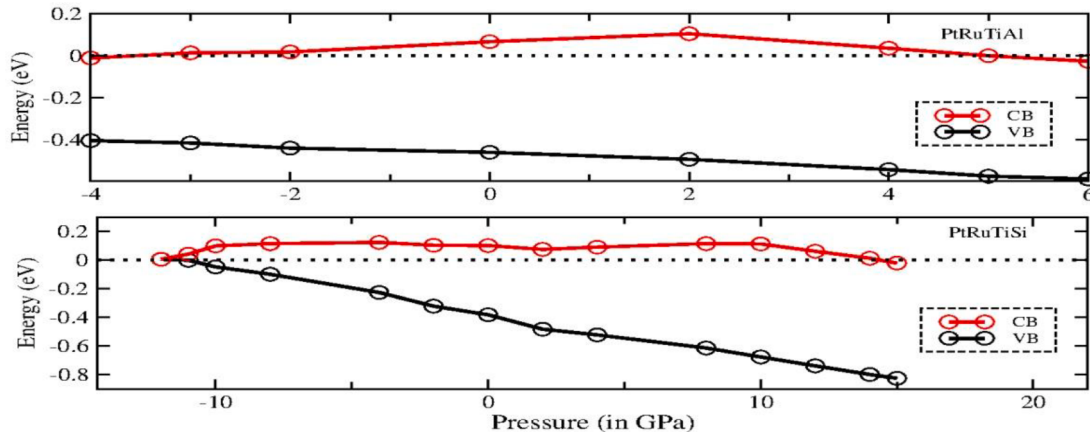


Fig. 8. Variation of conduction band energy (CB) along with valence band energy (VB) against applied pressure for PtRuTiAl (top) and PtRuTiSi (bottom).

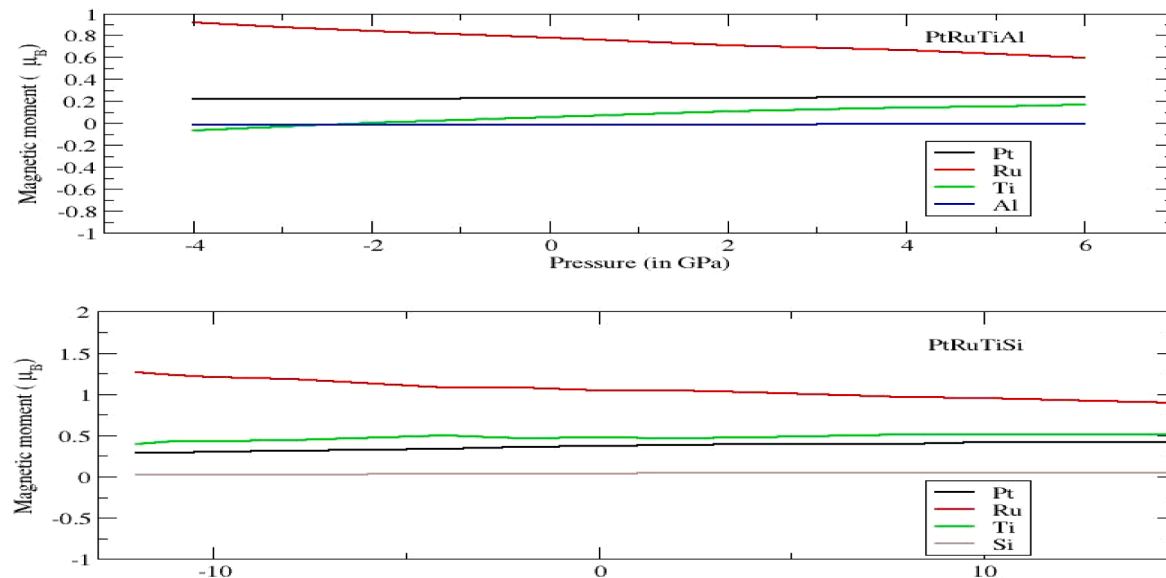


Fig. 9. Variation of magnetic moments of individual constituent members (Pt, Ru, Ti, and Al /Si) against the applied pressure.

properties to retain its half metallicity. It is also worth mentioning that PtRuTiSi has more excellent retention in half metallicity compared to the reported Heusler compounds like ScFeRhP [37] and CoRuTiSn [53]. Also, compared with the likes of reported materials like FeRuCrSi [41], FeRhCrSi, and FePdCrSi [54], the half-metallic retention beyond 5.8 Å is also preserved by PtRuTiSi. On the other hand, with lower calculated B and G, PtRuTiAl has a comparatively lower capacity in holding the half-metallic nature compared to PtRuTiSi. However, the HM nature cannot be ruled out near the pressure range of 4 GPa for PtRuTiAl.

The effect on the magnetic moment under the strenuous environment can be visualized in Fig. 9.

The magnetic moment is  $\sim 1 \mu_B/\text{f.u}$  (PtRuTiAl) and  $2 \mu_B/\text{f.u}$  (PtRuTiSi), which comply with the SP rule of  $M_T = Z_T - 24$  within the pressure range from -3 GPa to 4 GPa (PtRuTiAl) and -11 GPa to 14 GPa (PtRuTiSi). Considering the transition metals that govern the Heusler alloys' half-metallic nature, we find both the material showing an increase in the individual magnetic moment for Pt and Ti. In contrast, a relative decrement for Ru within the applied pressure range maintains the half-metallicity.

#### 4. Conclusion

A detailed *ab initio* study of PtRuTiZ (Z = Al and Si) shows 100 % spin polarisation at the Fermi energy level in the equilibrium lattice constant of 6.169 Å and 6.136 Å for PtRuTiAl and PtRuTiSi respectively. Both materials show thermodynamic and chemical stability. The mechanical properties show that PtRuTiSi is relatively more rigid and stiffer than PtRuTiAl due to higher bulk modulus and Young's modulus. The electronic study shows the materials to be sensitive in the GGA + U calculations and their compliance to the SP rule of  $M_T = Z_T - 24$ , giving the required magnetic moment of  $1 \mu_B/f.u$  and  $1.99 \mu_B/f.u$  for PtRuTiAl and PtRuTiSi respectively for its half-metallic character. The magnetic properties show its ferromagnetic profile, where Ru has the maximum contribution to the total magnetic moment. The material PtRuTiSi has more excellent retention keeping its HM nature within the pressure range from -11 to 14 GPa. The materials under study predicted to be half-metallic have a more significant potential to be used in the power devices in the field of spintronic.

#### CRediT authorship contribution statement

**Kunal Labar:** Data curation, Formal analysis, Investigation. **A. Shankar:** Project administration, Methodology, Software. **M. Das:** Validation, Visualization, Writing – original draft. **Ranjan Sharma:** Writing – review & editing, Supervision.

#### Declaration of Competing Interest

The authors declare that they have no known competing financial interests or personal relationships that could have appeared to influence the work reported in this paper.

#### Data availability

Data will be made available on request.

#### Acknowledgments

A.S. acknowledges a research grant to support the use of the computational facility from SERB, New Delhi, India (EEQ/2017/000319).

#### Data Availability

Data that support the findings obtained in this study are available from the corresponding author upon reasonable request.

#### References

- [1] K. Elphick, W. Frost, M. Samiepour, T. Kubota, K. Takanashi, H. Sukegawa, S. Mitani, A. Hirohata, Heusler alloys for spintronic devices: review on recent development and future perspectives, *Sci. Technol. Adv. Mater.* 22 (2021) 235–271.
- [2] H. Sukegawa, S. Kasai, T. Furubayashi, S. Mitani, K. Inomata, Spin-transfer switching in an epitaxial spin-valve nanopillar with a full-Heusler Co<sub>2</sub>FeAl<sub>0.5</sub>Si<sub>0.5</sub> alloy, *Appl. Phys. Lett.* 96 (2010), 042508.
- [3] I. Galanakis, K. Özdogan, E. Şaşoğlu, High-T C fully compensated ferrimagnetic semiconductors as spin-filter materials: the case of CrVXAl (X= Ti, Zr, Hf) Heusler compounds, *J. Phys.: Condens. Matter* 26 (2014).
- [4] R. Farshchi, M. Ramsteiner, Spin injection from Heusler alloys into semiconductors: A materials perspective, *J. Appl. Phys.* 113 (2013) p. 7.1.
- [5] Y. Feng, Z. Cheng, X. Wang, Substantial non-equilibrium tunnel magnetoresistance ratio in CoRhMnGe-based magnetic tunnel junction by interface modification, *Front. Chem.* 7 (2019) 550.
- [6] L. Bainsla, K.G. Suresh, Equiatomic quaternary Heusler alloys: A material perspective for spintronic applications, *Appl. Phys. Rev.* 3 (2016), 031101.
- [7] L. Hao, P. Cheng, R. Khenata, P.F. Liu, X. Wang, T. Yang, Complete spin gapless semiconductivity in equiatomic quarterary Heusler material TiZrMnAl, *J. Magn. Magn. Mater.* 508 (2020), 166880.
- [8] S.A. Khandy, J.D. Chai, Thermoelectric properties, phonon, and mechanical stability of new half-metallic quaternary Heusler alloys: FeRhCrZ (Z= Si and Ge), *J. Appl. Phys.* 127 (2020).
- [9] X. Liu, L. Li, Y. Cui, J. Deng, X. Tao, A nonmagnetic topological Weyl semimetal in quaternary Heusler compound CrAlTiV, *Appl. Phys. Lett.* 111 (2017), 122104.
- [10] D. Rani, K.G. Suresh, A.K. Yadav, S.N. Jha, D. Bhattacharyya, M.R. Varma, A. Alam, Structural, electronic, magnetic, and transport properties of the equiatomic quaternary Heusler alloy CoRhMnGe: Theory and experiment, *Phys. Rev. B* 96 (2017), 184404.
- [11] S. Idrissi, S. Ziti, H. Labrim, L. Bahmad, A. Benyoussef, Large Curie temperature and robust half metallicity of the CoRhMnSi equiatomic quaternary Heusler alloy, *Ferroelectrics* 582 (1) (2021) 36–45.
- [12] K. Özdogan, E. Şaşoğlu, I. Galanakis, Slater-Pauling behavior in LiMgPdSn-type multifunctional quaternary Heusler materials: Half-metallicity, spin-gapless and magnetic semiconductors, *J. Appl. Phys.* 113 (2013), 193903.
- [13] K. Chinnadurai, B. Natesan, First-principles calculations of 3d–4d transition metal-based LiMgPdSn-type FeCrRuZ (Z= Al, Ga, In, Si) equiatomic quaternary Heusler alloys, *Comput. Mater. Sci.* 188 (2021), 110116.
- [14] Y.C. Gao, X. Gao, The half-metallicity of LiMgPdSn-type quaternary Heusler alloys FeMnScZ (Z= Al, Ga, In): a first-principle study, *AIP Adv.* 5 (2015), 057157.
- [15] V. Aljiani, S. Ouardi, G.H. Fecher, J. Winterlik, S.S. Naghavi, X. Kozina, G. Stryganyuk, C. Felser, E. Ikenaga, Y. Yamashita, S. Ueda, K. Kobayashi, *Phys. Rev. B* 84 (2011), 224416.
- [16] S. Berri, M. Ibrir, D. Maouche, M. Attallah, Robust half-metallic ferromagnet of quaternary Heusler compounds ZrCoTiZ (Z= Si, Ge, Ga, and Al), *Comput. Condens. Matter* 1 (2014) 26–31.
- [17] J.P. Perdew, K. Burke, M. Ernzerhof, Perdew, burke, and ernzerhof reply, *Phys. Rev. Lett.* 80 (1998) 891.
- [18] I. Galanakis, P.H. Dederichs, N.J.P.R.B. Papanikolaou, Origin and properties of the gap in the half-ferrimagnetic Heusler alloys, *Phys. Rev. B* 66 (2002), 134428.
- [19] S. Idrissi, S. Ziti, H. Labrim, L. Bahmad, I.E.L. Housni, R. Khalladi, S. Mtougui, N. El Mekkaoui, Half-metallic behavior and magnetic proprieties of the quaternary Heusler alloys YFeCrZ (Z=Al, Sb and Sn), *J. Alloy. Compd.* 820 (2020), 153373.
- [20] A. Deb, Y. Sakurai, Electronic structure of the Cu<sub>2</sub>MnAl Heusler alloy, *J. Phys. Condens. Matter* 12 (2000) 2997–3012.
- [21] S.L. Dudarev, G.A. Botton, S.Y. Savrasov, C.J. Humphreys, A.P. Sutton, *Phys. Rev. B* 57 (1998) 1505.
- [22] S.A. Tolba, K.M. Gameel, B.A. Ali, H.A. Almossalam, N.K. Allam, The DFT+U: Approaches, accuracy, and applications, *Density Functional Calculations-Recent Progresses of Theory and Application*. 1 (2018) 5772.
- [23] D.P. Rai, A. Shankar, M.P. Ghimire, R.K. Thapa, In a comparative study of a Heusler alloy Co<sub>2</sub>FeGe using LSDA and LSDA+ U, *Phys. B: Condensed Matter* 407 (2012) 3689–3693.
- [24] S. Yousuf, D.C. Gupta, Insight into electronic, mechanical and transport properties of quaternary CoVTiAl: spin-polarized DFT+ U approach, *Mater. Sci. Eng. B* 221 (2017) 73–79.
- [25] R. Paudel, J. Zhu, Investigation of half-metallicity and magnetism of (Ni/Pd/Ru) ZrTiAl quaternary Heusler alloys for spintronic applications, *Physica B: Condens. Matter* 557 (2019) 45–51.
- [26] S.A. Khandy, First-principles understanding of structural electronic and magnetic properties of new quaternary Heusler alloy: FeVRuSi, *Mater. Res. Express* 5 (2018), 056516.
- [27] M. Zafar, H. Sadia, M. Rizwan, H. Arshad, S. Ahmad, S.S.A. Gillani, C.C. Bao, X. P. Wei, M. Shakil, Theoretical study of the structural, electronic, and magnetic properties of equiatomic quaternary CoTeCrZ (Z= Si, Ge, P) Heusler alloys, *Chin. J. Phys.* 64 (2020) 123–137.
- [28] M. Mushtaq, S. Khalid, M.A. Sattar, R. Khenata, T. Seddik, S.A. Dar, I. Muhammad, S.B. Omran, Electronic band structure, phase stability, magnetic and thermoelectric characteristics of the quaternary Heusler alloys CoCuZrAs and CoRhMoAl: Insights from DFT computations, *Inorg. Chem. Commun.* 124 (2021), 108384.
- [29] J. Nag, D. Rani, K.G Suresh A. Alam, Structural, magnetic, and electronic properties of equiatomic quaternary Heusler alloy CoRhTiAl. In *AIP Conference Proceedings* (Vol. 2265, No. 1, p. 030551). AIP Publishing LLC, 2020.
- [30] Y. Venkateswara, D. Rani, K.G. Suresh, A. Alam, Half-metallic ferromagnetism and Ru-induced localization in quaternary Heusler alloy CoRuMnSi, *J. Magn. Magn. Mater.* 502 (2020), 166536.
- [31] P. Blaha, K. Schwarz, G.K.H. Madsen, D. Kvásnica, J. Luitz, WIEN2k, An Augmented Plane Wave Plus Local Orbitals Program for Calculating Crystal Properties, Vienna University of Technology, Austria, 2001.
- [32] J.D. Pack, H.J. Monkhorst, “Special points for Brillouin-zone integrations”—a reply, *Phys. Rev. B* 16 (1977) 1748.
- [33] W. Setyawan, R.M. Gaume, S. Lam, R.S. Feigelson, S. Curtarolo, High-throughput combinatorial database of electronic band structures for inorganic scintillator materials, *ACS Comb. Sci.* 13 (2011) 382–390.
- [34] F.D. Murnaghan, The compressibility of media under extreme pressures, in: *Proceedings of the National Academy of Sciences*, 1944 (vol. 30), p. 244–247.
- [35] S.A. Khandy, J.D. Chai, Robust stability, half-metallic ferrimagnetism and thermoelectric properties of new quaternary Heusler material: A first-principles approach, *J. Magn. Magn. Mater.* 502 (2020), 166562.
- [36] A. Amudhavalli, R. Rajeswarapalanichamy, K. Iyakutti, First-principles study on Fe-based ferromagnetic quaternary Heusler alloys, *J. Magn. Magn. Mater.* 441 (2017) 21–38.
- [37] Z. Chen, H. Rozale, Y. Gao, H. Xu, Strain Control of the Tunable Physical Nature of a Newly Designed Quaternary Spintronic Heusler Compound ScFeRhP, *Appl. Sci.* 8 (2018) 1581.

- [38] V. Alijani, S. Ouardi, G.H. Fecher, J. Winterlik, S.S. Naghavi, X. Kozina, G. Stryganyuk, C. Felser, E. Ikenaga, Y. Yamashita, S. Ueda, Electronic, structural, and magnetic properties of the half-metallic ferromagnetic quaternary Heusler compounds CoFeMn Z (Z= Al, Ga, Si, Ge), Phys. Rev. B 84 (2011), 224416.
- [39] S. Idrissi, S. Ziti, H. Labrim, R. Khalladi, S. Mtougui, N. El Mekkaoui, I. Housni, L. Bahmad, Magnetic properties of the Heusler compound CoFeMnSi: Monte Carlo simulations, Phys. A: Statist. Mech. Appl. 527 (2019), 121406.
- [40] Q. Gao, I. Opahle, H. Zhang, High-throughput screening for spin-gapless semiconductors in quaternary Heusler compounds, Phys. Rev. Mater. 3 (2019), 024410.
- [41] X. Wang, H. Khachai, R. Khenata, H. Yuan, L. Wang, W. Wang, A. Bouhemadou, L. Hao, X. Dai, R. Guo, G. Liu, Structural, electronic, magnetic, half-metallic, mechanical, and thermodynamic properties of the quaternary Heusler compound FeCrRuSi: a first-principles study, Sci. Rep. 7 (2017) 1–13.
- [42] Y. Han, X. Wang, First-Principles Investigation of Half-Metallic Ferromagnetism of a New 1:1:1 Type Quaternary Heusler Compound YRhTiSi, J. Supercond. Nov. Magn. 32 (2019) 1681–1689.
- [43] Y. Le Page, P. Saxe, Symmetry-general least-squares extraction of elastic data for strained materials from ab initio calculations of stress, Phys. Rev. 65 (2002), 104104.
- [44] S.C. Wu, S.S. Naghavi, G.H. Fecher, C. Felser, A critical study of the elastic properties and stability of Heusler compounds: phase change and tetragonal  $X_2YZ$  compounds, J. Mod. Phys. 9 (2018) 775.
- [45] M. Born, K. Huang, Dynamical theory of crystal lattices, 72, Clarendon Press, Oxford, 1954.
- [46] W. Everhart, J. Newkirk, Mechanical properties of Heusler alloys. Heliyon 5 (2019) e01578.
- [47] M.I. Khan, H. Arshad, M. Rizwan, S.S.A. Gillani, M. Zafar, S. Ahmed, M. Shakil, Investigation of structural, electronic, magnetic and mechanical properties of a new series of equiatomic quaternary Heusler alloys CoYCrZ (Z= Si, Ge, Ga, Al): a DFT study, J. Alloy. Compd. 819 (2020), 152964.
- [48] M. Benkabou, H. Rached, A. Abdellaoui, D. Rached, R. Khenata, M.H. Elahmar, B. Abidi, N. Benkhetou, S. Bin-Omran, Electronic structure and magnetic properties of quaternary Heusler alloys CoRhMnZ (Z= Al, Ga, Ge, and Si) via first-principle calculations, J. Alloy. Compd. 647 (2015) 276–286.
- [49] H.L. Huang, J.C. Tung, H.T. Jeng, A first-principles study of rare earth quaternary Heusler compounds: RXVZ (R= Yb, Lu; X= Fe Co, Ni; Z= Al, Si), PCCP 23 (2021) 2264–2274.
- [50] S.A. Khandy, J.D. Chai, Thermoelectric properties, phonon, and mechanical stability of new half-metallic quaternary Heusler alloys: FeRhCrZ (Z= Si and Ge), J. Appl. Phys. 127 (2020), 165102.
- [51] Z. Hu, H. Metiu, Choice of U for DFT+ U calculations for titanium oxides, J. Phys. Chem. C 115 (2011) 5841–5845.
- [52] D. Garrido-Diez, I. Baraia, May, Review of wide bandgap materials and their impact in new power devices, 2017 IEEE International workshop of electronics, control, measurement, signals, and their Application to Mechatronics (ECMSM), IEEE, p.1–6.
- [53] S. Bahramian, F. Ahmadian, Half-metallicity, and magnetism of quaternary Heusler compounds CoRuTiZ (Z= Si, Ge, and Sn), J. Magn. Magn. Mater. 424 (2017) 122–129.
- [54] L. Feng, J. Ma, Y. Yang, T. Lin, L. Wang, The electronic, magnetic, half-metallic, and mechanical properties of the equiatomic quaternary Heusler compounds FeRhCrSi and FePdCrSi: A first-Principles Study, Appl. Sci. 8 (2018) 2370.
- [55] E.C. Stoner, Collective electron ferromagnetism, Proc. R. Soc. Lond. A 165 (1938) 372–414.
- [56] R.K. Guo, G.D. Liu, T.T. Lin, W. Wang, L.Y. Wang, X.F. Dai, The electronic, structural and magnetic properties of Heusler compounds ZrCrCoZ (Z= B, Al, Ga, In): A first-principles study, Solid State Commun. 270 (2018) 111–118.
- [57] H. Zhang, W. Liu, T. Lin, W. Wang, G. Liu, Phase Stability and Magnetic Properties of Mn<sub>3</sub>Z (Z= Al, Ga, In, Ti, Ge, Sn, Pb) Heusler Alloys, Appl. Sci. 9 (2019) 964.